Reservoir properties of fault-related hydrothermally altered granites in Cornwall: Implications for geothermal energy prospectivity

Nathaniel Forbes Inskip[1], Nick Harpers[1], Robin Shail[2], Hannes Claes[3], Sabine den Hartog[1], Andreas Busch[1]

[1] The Lyell Centre, Heriot-Watt University, Edinburgh, UK

[2] Camborne School of Mines, University of Exeter, Penryn, UK

[3] KU Leuven, Department of Earth and Environmental Sciences, Celestijnenlaan 200E, BE-3001, Leuven, Belgium

Corresponding author email address: n.forbes_inskip@hw.ac.uk

Abstract

Granite based geothermal systems are currently being explored in Cornwall for their potential to decarbonise energy production. Fault structures, known locally as cross-courses, are being targeted due to their potential to both host fluids at depth and create zones of enhanced permeability through fault related fractures. These structures have been transmissive in the past, evidenced by mineral veins, and surrounding host rock alteration. Hydrothermal alteration has the potential to affect the petrophysical properties of a rock, however these effects on potential geothermal systems has received little attention to date. In this study we measure the tensile strength, porosity and permeability of samples of Carnmenellis Granite which have been hydrothermally altered to different amounts. We find that hydrothermal (argillic) alteration leads to a weaker, more porous and permeable rock, which has implications both in terms of reservoir volumes and fluid production rates. The alteration of feldspars into clay minerals leads to microporous regions that are connected throughout the material, and consequently an increase in total porosity by an order of magnitude and matrix permeability by up to 4 orders of magnitude. However, fractures hosted in the altered material are more likely to close under higher effective stress than those hosted in comparatively unaltered material, which leads to a lower fracture permeability. Finally, we demonstrate that hydrothermally altered zones have the potential to host significantly greater amounts of accessible fluid than the fractures alone, and that they should be considered when assessing reservoir volumes in these types of geothermal systems.

1. Introduction

Geothermal energy is one of the few low carbon renewable energy technologies that can provide a continuous supply of energy, both heat and power, and so contribute to baseload demand. Historically, geothermal energy development has been confined largely to areas near plate boundaries or active volcanism, where local geothermal gradients are particularly high, and high temperature fluids (>200°C) are accessible within the shallow subsurface (<3 km depth) (Harvey *et al.* 2016). However, High-Heat Producing Granites (HHPGs) provide an opportunity for geothermal power production away from plate boundaries. HHPGs contain high concentrations of uranium, thorium and potassium, which undergo radioactive decay and so give off heat (Busby *et al.* 2015; Artemieva *et al.* 2017; Busby and Terrington 2017; Mccay and Younger 2017; Gluyas *et al.* 2018). In the UK the average geothermal gradient is ~26°C/km (Busby 2010), as it is far away from any active plate boundary or active volcanism. However, in areas that contain HHPGs, the geothermal gradient often

exceeds this, for example in Cornwall, where local geothermal gradients can exceed 35°C/km (Beamish and Busby 2016).

The potential for geothermal energy development in Cornwall has been known for many years (Rollin 1982; Pine and Batchelor 1984; Busby 2010; Beamish and Busby 2016; Busby and Terrington 2017; Batchelor *et al.* 2020), and in the 1970-80s Rosemanowes Quarry was the site of the Hot Dry Rock (HDR) Project (Pine and Batchelor 1984; Parker 1999). Here a series of wells were drilled and hydraulically stimulated within the Carnmenellis Granite to assess the likelihood of creating and improving permeability at depth. Two of the main findings were that: 1) an elevated geothermal gradient exists locally, and 2) that existing fracture networks can be permeable at depth. Despite these results, the interest in geothermal energy in the UK diminished in favour of other cheaper energy sources (Gluyas *et al.* 2018). Recently there has been a renewed impetus to deep geothermal energy development in Cornwall, with two projects having drilled wells to depths of ~5 km and recorded bottom hole temperatures over 190°C. The two projects are the United Downs Deep Geothermal Power (UDDGP) project and the Eden project (Batchelor *et al.* 2020). While there are differences in the granite types being targeted for these projects, the play type is similar in both (Figure 1).

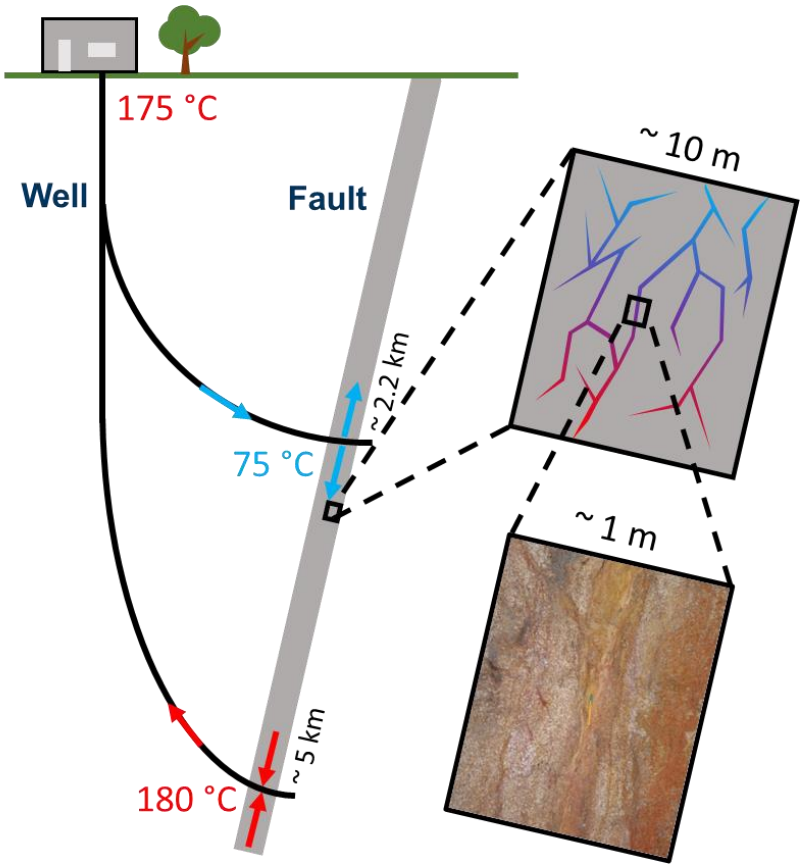

Figure 1: Schematic of geothermal system at UDDGP, modified after (Ledingham *et al.* 2019). The photograph was taken from a fault zone at Holman's Test Mine, 1.5 km SE of Camborne (Cornwall, UK), where samples for this study were collected.

Granites are known to have very low porosities and matrix permeabilities, and therefore a well-connected fracture network is required to host and transmit fluids through the rock (Abesser *et al.* 2020). This fracture network needs to be intersected by both producer and injector wells for a project to be economically viable. Although fractures are common in the subsurface, predicting their properties such as length, aperture, connectivity and permeability is non-trivial. Faults often contain pervasive, well-connected fracture networks in their damage zone (Faulkner *et al.* 2010), and the two projects in Cornwall aim to exploit these fracture networks to transmit fluids (Figure 1). The faults that are being targeted are the Porthtowan Fault Zone within the Carnmenellis Granite (UDDGP) (Ledingham *et al.* 2019) and the Great Cross-course within the St Austell Granite (Eden) (Eden Geothermal Limited 2023). Both are examples of the 'cross-course' fault zones that occur throughout SW England. These typically strike NW-SE to N-S (with a subordinate conjugate NNE-SSW set) and their name is derived from a typical high angle intersection with, and displacement of, granite-related magmatic-hydrothermal veins hosting W-Sn-Cu-Zn mineralisation (e.g. Dines 1956; Dearman 1963).

Cross-course fault zones have a complex evolution involving multiple episodes of reactivation. Some initiated, within the pre-granite host rocks, as strike-slip transfer faults during NNW-SSE Variscan thrusting (Carboniferous). These same fault zones also acted as strike-slip transfer faults during the immediate post-Variscan NNW-SSE extensional regime that controlled granite generation and emplacement, and magmatic-hydrothermal W-Sn-Cu-Zn mineralisation (Early- to Mid-Permian) (Shail and Alexander 1997). Faults of this orientation propagated from the host rocks into the granites during this episode. Regional late Permian to Triassic ENE-WSW extension resulted in extensional reactivation of NNW-SSE striking fault zones, the growth of new extensional faults, and substantial migration of epithermal basinal brines that is manifested in granites by, respectively, the occurrence of quartz/chalcedony ± siderite/hematite veins and kaolinised/hematised wall rocks (Chadwick and Evans 1995; Shail and Alexander 1997; Gleeson *et al.* 2000). During Cenozoic N-S intraplate shortening, strike-slip reactivation of cross-course fault zones occurred throughout SW England (Dearman 1963; Holloway and Chadwick 1986).

Mineralisation along fractures and adjacent hydrothermal alteration attest to cross-course fault zones possessing at least transient permeability that has controlled multiple episodes of paleogeothermal fluid migration, including hydrocarbons (Baba *et al.* 2018). Nevertheless, mineralisation and hydrothermal alteration can affect the present-day transport properties (Staněk and Géraud 2019). In the context of geothermal energy projects these processes are therefore key to determine project viability. Though this has been investigated by some authors (Stimac *et al.* 2015; Mayer *et al.* 2016; Mordensky *et al.* 2018; Heap *et al.* 2019; Staněk and Géraud 2019), our understanding of the implications of these processes on geothermal energy systems remains poor. For example, a reservoir can often become compartmentalised by mineralised fractures (Gudmundsson 2011; Moore and Wade 2013) or permeability may be drastically reduced through the conversion of feldspars to clay minerals (Heap *et al.* 2019). Alternatively, the alteration process may enhance porosity and permeability by dissolution and loss of alteration products (Nishimoto and Yoshida 2010; Mayer *et al.* 2016).

Our study aims to investigate and improve our understanding of how both hydrothermal alteration and the presence of fractures affect the reservoir properties of the Carnmenellis Granite. It is therefore directly relevant for the UDDGP project, but also for other similar granite-based geothermal systems. We conducted a series

of experiments on both fractured and intact granite samples of different alteration grade and measured their porosity and permeability. We further investigate potential reasons for the permeability behaviour by analysing sample composition and structure using scanning electron microscopy (SEM), optical microscopy, and X-ray computer tomography (XCT).

2. Sample material

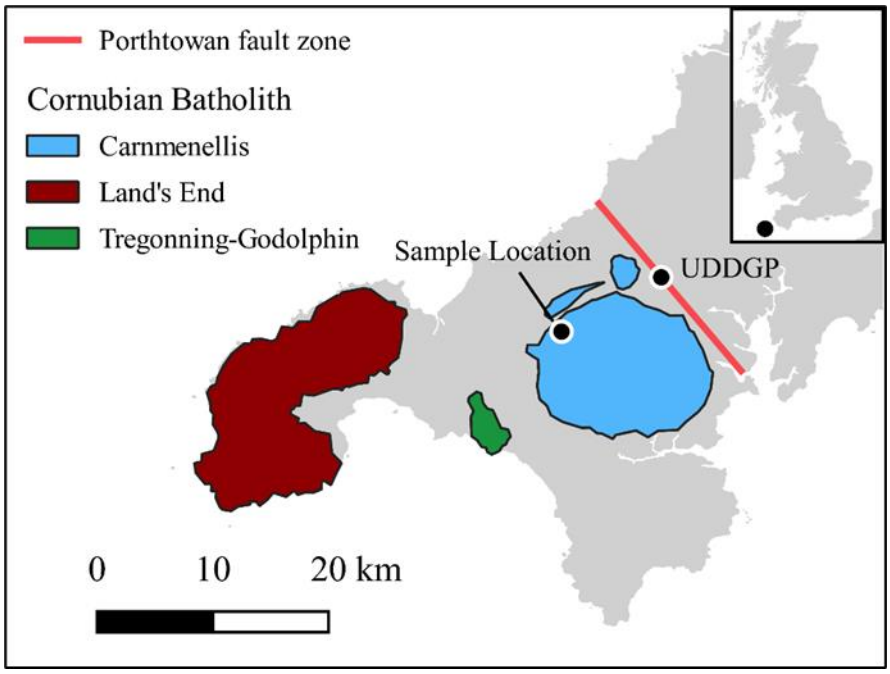

Figure 2: Map of south-west Cornwall (England) indicating the locations of three major plutons. The plutons are part of the Cornubian Batholith that was emplaced during Early Permian post-collisional extension. The map shows the sampling location (Holman's Test Mine) and trace of the Porthtowan Fault Zone (modified after Simons et al. (2016)).

Granite samples were collected from the Carnmenellis pluton in SW Cornwall, England. The pluton is part of the Cornubian Batholith that spans from the Isles of Scilly in the SW to the Dartmoor pluton in the NE (Bott et al., 1958). The batholith was emplaced during Early Permian post-collisional extension and the upper parts of the Carnmenellis pluton was dated to 293.7 ± 0.6 Ma ago (Chesley et al., 1993). Due to the lithophile behaviour of radioactive elements like uranium and thorium, granite bodies often contain higher concentration of these elements relative to the surrounding host rock. The decay of these elements causes enhanced heat flow which, in the case of Cornwall, is close to double the UK average (Busby and Terrington 2017). The Carnmenellis Granite is a two-mica (biotite-muscovite) granite; it is medium- to coarse-grained and contains K-feldspar phenocrysts (< 25 mm) that make up <5 to 25 wt% of the rock (Simons *et al.* 2016).

The granite samples used in this study have been collected from the Holman's Test Mine which is located about 1.5 km SE of Camborne and reaches depths of approximately 30 m from the present-day surface within the Carnmenellis Granite (Figure 2). The mine was chosen as a source for sample material because the rock in the mine has undergone a lower degree of alteration by weathering compared to surface samples. The granite within Holman's Test Mine hosts multiple steeply-inclined quartz-tourmaline-chlorite veins that formed during magmatic-hydrothermal mineralisation and these are post-dated by minor cross-course fault zones that

host quartz ± hematite veins and are accompanied by wall-rock kaolinisation (Figure 3). We consider these structures to be an appropriate small-scale analogue for investigating processes that influence permeability relevant for geothermal energy projects in Cornwall.

Figure 3: Minor cross-course fault zone hosted by the Carnmenellis Granite within the Holman's Test Mine. The fault zone include quartz ± hematite veins and wall-rock kaolinisation and crosscuts earlier quartz-tourmaline-chlorite mineral veins that formed during granite-related mineralisation. The pen is placed in the fault core for scale.

Faults can act as either barriers or channels for fluid flow in rocks (Gudmundsson 2011). In crystalline rocks like granites, they are required to enable economical fluid production for a geothermal system. Hydrothermal fluids flowing along the fault promote geochemical alteration of the host rock. The rock is gradually less altered the further it is located from the fault core (Nishimoto and Yoshida 2010) due to a reduction in flow paths (fractures) further away from the main structure (Faulkner *et al.* 2010). We investigate the alteration along the cross-courses in Holman's Test Mine as proxy for alteration in the Porthtowan Fault Zone at depth. Our samples were collected to capture and characterise the different natural geochemical alteration stages of the granite.

The three samples analysed in this paper (Figure 4) are cohesive and medium-grained and were chosen to represent progressive natural hydrothermal alteration. We have therefore termed these samples 'unaltered', 'slightly altered', and 'highly altered' granite.

X-ray diffraction compositional analysis of the 'unaltered' granite' (Table 1) indicates quartz (31 wt%), K-feldspar (28 wt%), and plagioclase (20 wt%), amounts typical for a pristine granite, while it contains only a very low amount of secondary clays (3 wt% kaolinite+chlorite+smectite) in addition to the primary muscovite and biotite (18 wt%). The sample shows no obvious alteration colours and was collected farthest from the fault core.

The 'slightly altered' granite contains thin tourmaline veins (2 wt%) and has a light brown colour. It contains similar amounts of quartz and feldspars as the unaltered granite but shows incipient chloritisation (5 wt% chlorite and smectite) and kaolinisation (2 wt% kaolinite) that account for the reduction in primary biotite and muscovite (12 wt%). Tourmaline veins are indicative of magmatic-hydrothermal mineralisation which occurred

during, or shortly after, pluton construction (Early Permian) (Chen *et al.* 1993) and pre-date the quartz veins developed in the cross-course fault zone (late Permian – Early Triassic). Nevertheless, they may also affect the mechanical and transport properties of the granite hosting them.

The 'highly altered' granite, has been degraded, primarily by the transformation of plagioclase feldspar into clays (argillic alteration). The sample was collected closest to the fault core to be sufficiently cohesive for plug preparation. More unconsolidated sample material was collected to investigate additional alteration states, but they were unsuitable for the experiments presented in this paper but are discussed in terms of friction properties in (Harpers et al. (2022).

Blocks of the three granites were used to prepare an intact (unfractured) and a fractured set of 1'' sample plugs for the three materials tested. The samples were then cut and ground to result in plugs of 0.5" length. The highly altered granite was too weak for coring, so disks were instead turned from a block of material using a lathe. We then measured the permeability of the unfractured samples to obtain matrix properties; permeability testing of the fractured samples followed Brazil disk testing (ISRM 1978; Ulusay 2014) using a deformation rate of 0.1 mm/min. The Brazil disk test is used to measure the indirect tensile strength of a sample (Table 1), and in doing so a Mode-I fracture which spans the sample is produced. The slightly altered granite has the highest tensile strength (15.30 ± 0.64 MPa), which is marginally higher than that of the unaltered granite (11.31 ± 1.33 MPa). The highly altered granite is significantly weaker than the other two materials (1.55 MPa).

NMR analyses were carried out on water-saturated samples with an in-house constructed fixed-field Halbach-based 0.23T rock core analyser at the Sakellariou NMR lab of the KU Leuven. T2s were measured by the Carr Purcell Meiboom Gill (CPMG) method (Carr and Purcell 1954; Meiboom and Gill 1958). After calibration, with known quantities of water and brine ($CuSO_4$), total porosity was estimated based on signal intensity and the proportional area under the T2 distribution curve. Simultaneously, Archimedes porosities, based on dry, saturated and submerged weights, were determined. The porosities, independent of the technique, of both the unaltered and slightly altered granite are broadly similar (1-2%), whereas the porosity of the highly altered sample is much higher (~10%).

Table 1: XRD results for granitic samples used in this study in wt%. After Warr (2021): Ms muscovite, Bt biotite, Ilt illite, Chl chlorite, Sme smectite.

Mineral (wt-%)	highly altered	slightly altered	unaltered
Quartz	37	30	31
Plagioclase	1	20	20
K-Feldspar	38	28	28
Ankerite	< 0.5	< 0.5	0
Anhydrite	< 0.5	< 0.5	0
Tourmaline	< 1	2.0	< 1
Ms+Bt+Ilt*	10	12	18
Kaolinite	7	2	1
Chl+Sme*	3	5	2
Unknown**	3	2	< 1
Tensile strength (MPa)	1.55	15.30 ± 0.64	11.31 ± 1.33
Porosity (%)	10.31	1.21	1.99

*Abbreviations after Warr (2021)

**Amorphous and not identifiable components

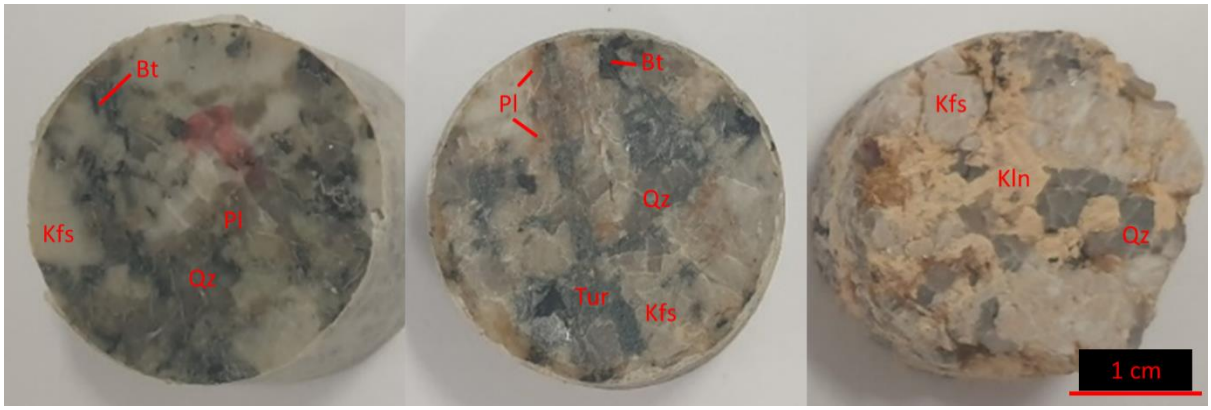

Figure 4: Sample disks from left 'unaltered', middle 'slightly altered', to right 'highly altered'. Note changes in colour due to alteration. The 'highly altered' sample was prepared in a lathe, while the other two were plugged using a coring drill. After Warr (2021): Pl plagioclase, Kfs K-feldspar, Qz quartz, Bt biotite, Tur tourmaline, Kln kaolinite.

3. Methods

3.1. Permeability

The permeability of both fractured and intact samples was measured using a *Dynchem* permeameter at the GeoEnergy Laboratories, Heriot-Watt University. Samples were tested using both the steady-state and non-steady state methods (Fink *et al.* 2017; Forbes Inskip *et al.* 2022). In both instances nitrogen was used as the permeating fluid, at a constant temperature of 25°C. Samples were placed in a Viton™ sleeve to stop the confining fluid (water) accessing the sample, before then being placed in a pressure vessel. Confining pressure was applied isotropically, via the confining fluid, while the permeating fluid (nitrogen) was introduced to the sample at one end of the sample at pressure (upstream) which then permeated through the sample towards the other end of the sample (downstream) which was at a lower pressure. The mean pore fluid pressure (P_p) was kept constant at 1 MPa, and the confining pressure (P_c) was varied in steps in order to derive a

permeability versus effective stress relationship for each sample tested. Here we consider the Terzaghi's effective stress relationship, i.e. $P_c - P_p$. The effective stresses that were tested in all experiments were 4, 9, 19, 29 and 34 MPa.

All fractured samples, but also the sample of intact highly altered granite were tested using the steady-state method, while the intact samples of slightly altered and unaltered granite were tested using the non-steady state method. Descriptions of both methods are given below, but it is necessary to use the non-steady state method if sample permeability is so low that it is not possible to reach a constant flow rate in a reasonable time frame (<several weeks) when using the steady state method. However, the apparatus is calibrated regularly using a ceramic plug of a known permeability, and the difference in results between the two methods is negligible. Unfortunately, due to operational problems during testing it was not possible to obtain reliable permeability data for an intact sample of unaltered granite.

Steady-state method

A mass flow controller was used to measure the mass flow of the permeating fluid through the sample, and experiments were continued until a constant mass flow rate was reached, thus satisfying the steady-state test requirements. We converted the mass flow rate into volumetric flow rate using the density of the fluid and the equation of state of the fluid at a 25°C (Span *et al.* 2000). We then calculated the sample permeability using Darcy's equation:

$$k = -\frac{Q \cdot \mu \cdot L}{A \cdot \Delta p}$$

where k is permeability [m^2], Q is volumetric flow rate [$m^3\ s^{-1}$], μ is viscosity [$Pa\ s^{-1}$], L is sample length [m], A is cross sectional area [m^2] and Δp is pressure difference [Pa].

Two loading and unloading cycles were carried out for each sample, starting at an effective stress of 4 MPa and working up to an effective stress of 34 MPa before decreasing the effective stress again back to 4 MPa and conducting the cycle again. A significant amount of hysteresis is observed between the first loading cycle and the subsequent cycles. This is commonly observed in such experiments (Cuss *et al.* 2017; Houben *et al.* 2020; Forbes Inskip *et al.* 2022), and is due to the sample being loaded from ambient pressure conditions in the first cycle. We omit data from this first loading cycle in the results and analysis that follow.

Non-steady state method

We use the non-steady state method where the permeability of a sample is so low that it requires a long period of time (>several weeks) to reach a constant flow rate required for the steady-state method. This method involves measuring the pressure decay of the permeating fluid over time within a known volume upstream, and simultaneous pressure increase with time within a known volume downstream. The slope of the $\ln(P_{up} - P_{down})$ vs time is calculated from this pressure data, which we denote as c.

The permeability is then calculated using the following equation:

$$k = -\frac{c \cdot \mu \cdot L}{A \cdot P_p \cdot z \cdot \left(\frac{1}{V_1} + \frac{1}{V_2}\right)}$$

where z is gas compressibility factor [-], V_1 is upstream volume [m^3] and V_2 is downstream volume [m^3].

We use a Klinkenberg correction to correct for slip flow (Klinkenberg 1941; Rushing *et al.* 2004; Fink *et al.* 2017). This allows us to obtain an equivalent liquid permeability for each effective pressure step, which is important when considering water/brine based geothermal systems like those in Cornwall. Due to the time constraints we were not able to measure the permeability of the intact sample of slightly altered granite at an effective stress of 34 MPa, and only one loading cycle was performed.

3.2. Image analysis

Samples were imaged and analysed using a combination of optical microscopy, Scanning Electron Microscopy (SEM) and micro-Computed Tomography (µ-CT). Image analysis was used to characterise the materials petrographically, and understand how the texture of the materials varies due to alteration processes. While microscopy can provide valuable information in 2D, it is not possible to use these techniques to analyse how pervasive alteration and fracturing is across a sample. We therefore use µ-CT image analysis to characterise samples in 3D.

Microscopy

Thin sections of the unaltered and highly altered granites were prepared using standard practice. This involved polished using standard mechanical means and the thin sections were not covered in order to conduct SEM analysis. A standard microscope was used to analyse the thin sections using both plane polarised and cross polarised light, while a Quanta 650 FEG SEM was used for the SEM analysis. Resolution of the SEM analysis is ~1.3 µm. Thin sections were not prepared of the slightly altered granite due to material availability.

µ-CT

Following the permeability experiments samples were scanned under ambient conditions using an EasyTom µ-CT Scanner, at the Rock Mechanics Laboratory at Heriot-Watt University, at a resolution of ~15 µm. The scans were denoised using a non-local means filter using Avizo (ThermoFisher Scientific) and then different minerals were identified using intensity thresholding, which describes the definition of phases based on grey-scale windows in the scan.

4. Results and discussion

Permeability of Intact samples

Figure 5 shows matrix permeability against effective stress for intact samples of the slightly altered and highly altered granites. The permeability of the highly altered material is up to four orders of magnitude higher than that of the slightly altered material. The data from both rock types fit a power law function well, which is common when plotting permeability against effective stress (Phillips *et al.* 2020).

The permeability of the slightly altered material at an effective stress of 29 MPa is slightly higher than at an effective stress of 19 MPa, which is unexpected. This is likely due to the fact that the measured values are near the limit of equipment permeability resolution (~10^{-21} m^2) and so any difference at this level may fall within the error of the measurement itself.

Although it was not possible to gather permeability data for an intact sample of unaltered granite, we assume that the permeability is similar to that of the slightly altered granite given the similarities in porosity and mineralogy.

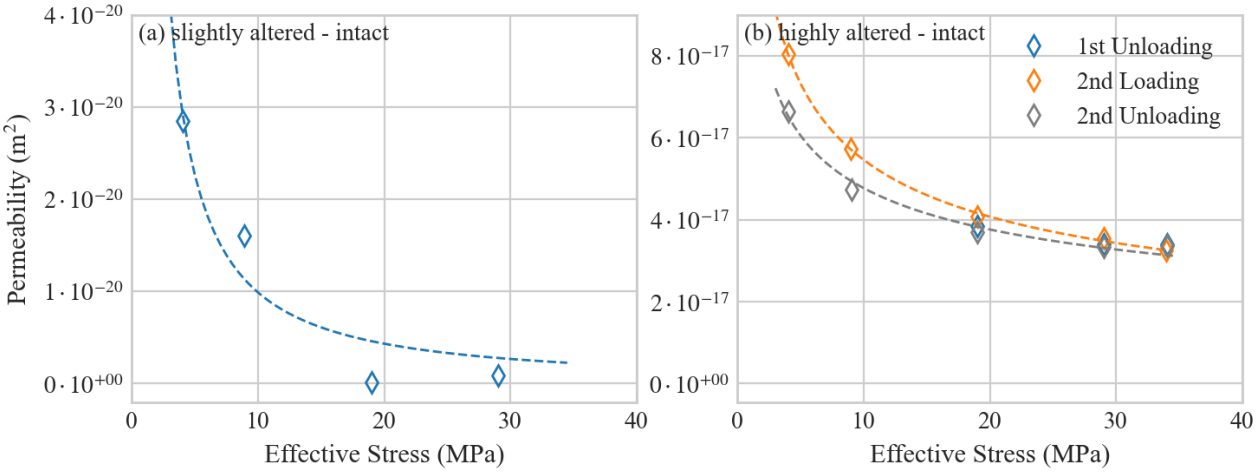

Figure 5: Permeability against effective stress relationship of intact Carnmenellis Granite samples.

Permeability of Fractured samples

Figure 6 shows permeability against effective stress data for fractured samples of all three rock types. Fluid flow comprises a matrix and fracture component. In low permeability rocks (e.g. crystalline rocks, mudrocks, shales) fluid flow will be dominated by the fracture component, but for more permeable rocks (e.g. porous sandstone and limestones) the contribution of the matrix is also important to consider. Fracturing increases the permeability of the slightly altered granite by over 4 orders of magnitude, and by about order of magnitude for the highly altered material.

The permeability of the fractured unaltered granite is up to half an order of magnitude higher than that of the slightly altered granite which itself is over an order of magnitude higher than that of the highly altered granite.

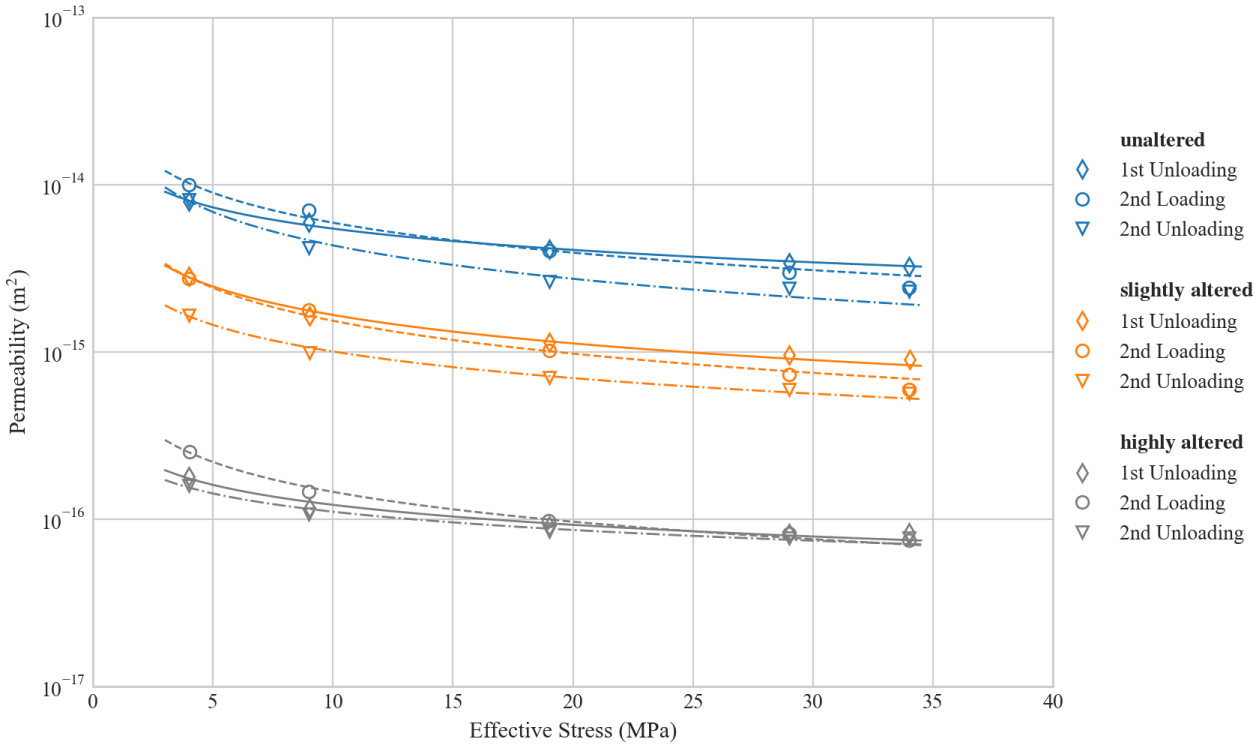

Figure 6: Permeability against effective stress for fractured samples Carnmenellis Granite.

Although the Brazil disk test method usually only produces a single throughgoing tensile fracture, it can sometimes create multiple throughgoing fractures. µ-CT analysis of the fractured samples used for this study reveal a second, "branch" fracture within the unaltered granite sample (Figure 7). This fracture also spans the whole thickness of the sample, and it therefore likely contributed to fluid flow during our experiments. In contrast, the slightly altered and highly altered granite samples contain some smaller scale fractures, most of which are largely or wholly contained within individual crystals (Figure 7), and therefore unlikely contributed to fluid flow across the sample.

Due to the similarities between the unaltered and slightly altered granites in terms of porosity and mineralogy, and given that the matrix permeability of the slightly altered material – and assumed unaltered material - is incredibly low (<1 x 10^{-20} m^2), we suggest that the difference in terms of permeability of the fractured samples of these two rock types is due to the contribution to flow through this branch fracture, rather than any difference in material properties.

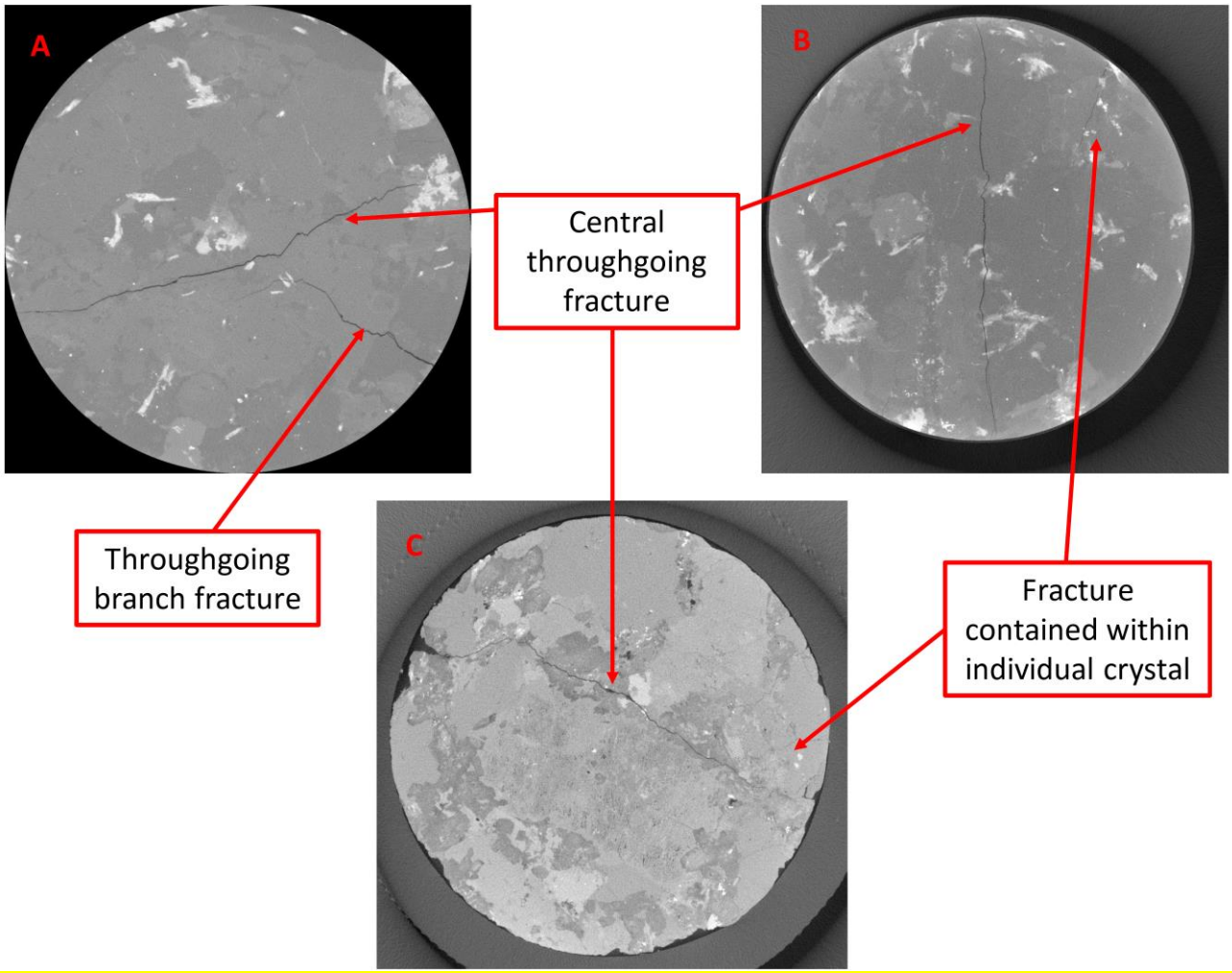

Figure 7: CT images of fractured samples of A) Unaltered Granite B) Slightly Altered Granite C) Highly Altered Granite. A central throughgoing fracture is observed in all three samples, but a throughgoing branch fracture is observed in the sample of Unaltered Granite. For the samples of Slightly Altered and Highly Altered Granite any other fractures are largely or wholly contained within individual crystals and do not span the thickness of the sample.

Textural controls on permeability

The results of this study demonstrate that there is not a significant difference in porosity and mineralogy between the unaltered and slightly altered granite. Although we were unable to produce reliable permeability data for the intact sample of unaltered granite, we assume that it would be comparable to the slightly altered granite (i.e. $<1 \times 10^{-20}$ m^2) due to these similarities, particularly in terms of very low porosity (<2%).

There are significant differences between the highly altered and the slightly altered - and we assume unaltered - granites in terms of matrix permeability. The main alteration process observed around cross-courses (and therefore our sample set) is argillic alteration, which describes the formation of clay minerals (kaolinite and smectite) at the expense of plagioclase (Bevins *et al.* 2010). The dissolution-precipitation replacement of plagioclase with microcrystalline and microporous clay aggregates is open system behaviour and increases rock porosity as some plagioclase components are lost in solution. Some clay particles may also be lost, increasing porosity further, and resulting in a relative increase in quartz (37 wt%) and K-feldspar (38 wt%)

relative to the unaltered / less altered granites. This can be seen in the thin section in both Figure 8 and Figure 9. Figure 9 shows a series of microscopy images (optical and SEM) of the highly altered material that focus on a clay rich region, i.e. the altereation products. In Figure 9d small (micro) pores are observed between the clay particles (i.e. intergranular porosity), which we suggest is the reason that the highly altered material has such a high porosity (~10%). By comparison, Figure 10 suggests that alteration of some minerals within the unaltered granite has started but it has not yet affected the rock composition significantly (Table 1). The unaltered granite contains almost no pores or fractures (see Figure 8), which supports the hypothesis that the matrix permeability is at least as low as the slightly altered granite.

The difference in matrix permeability of the slightly altered – and we assume unaltered - granite and the highly altered granite suggests that the 'pores' created through argillic alteration of the highly altered granite are connected throughout the sample, despite the process mainly affecting the plagioclase (20-35% of the unaltered rock mass).

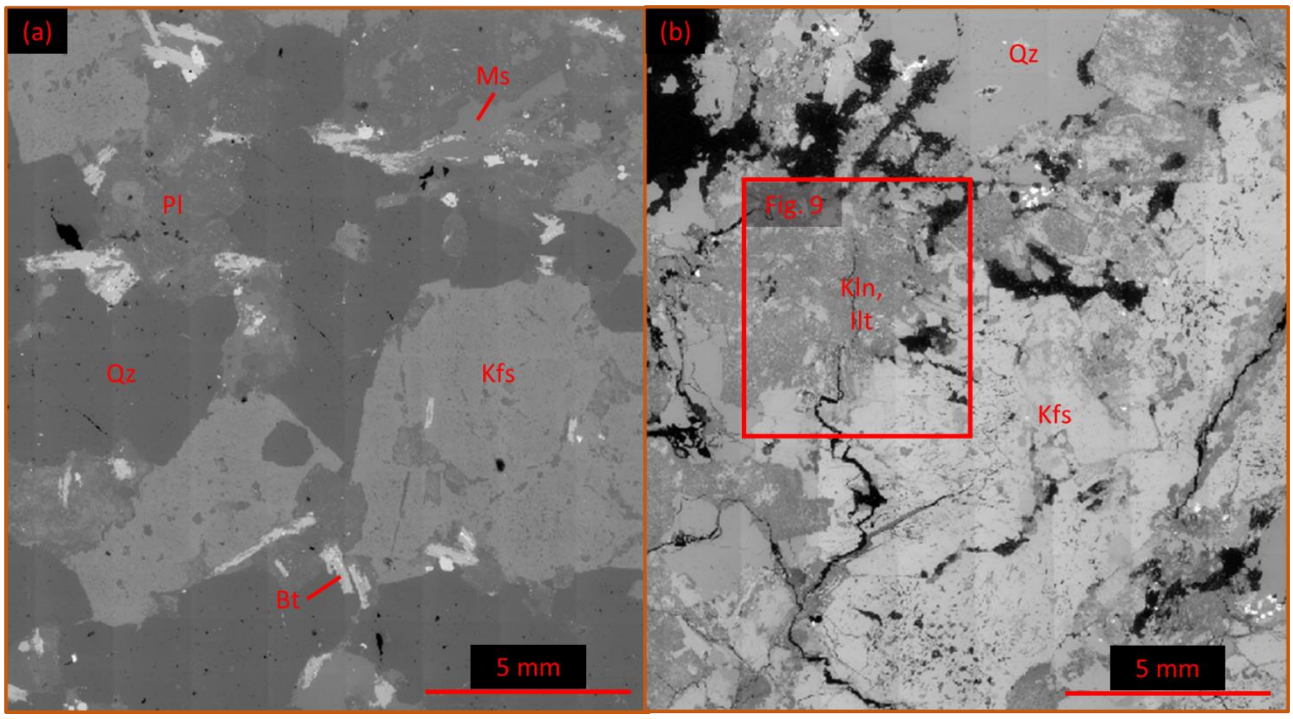

Figure 8: SEM images of (a) unaltered and (b) highly altered Carnmenellis Granite, which was used in this study. The red box indicates a region where a plagioclase has been fully altered into clays. This region is subject of Figure 9. After Warr (2021): Pl plagioclase, Kfs K-feldspar, Qz quartz, Bt biotite, Ms murcovite, Kln kaolinite, Ilt illite.

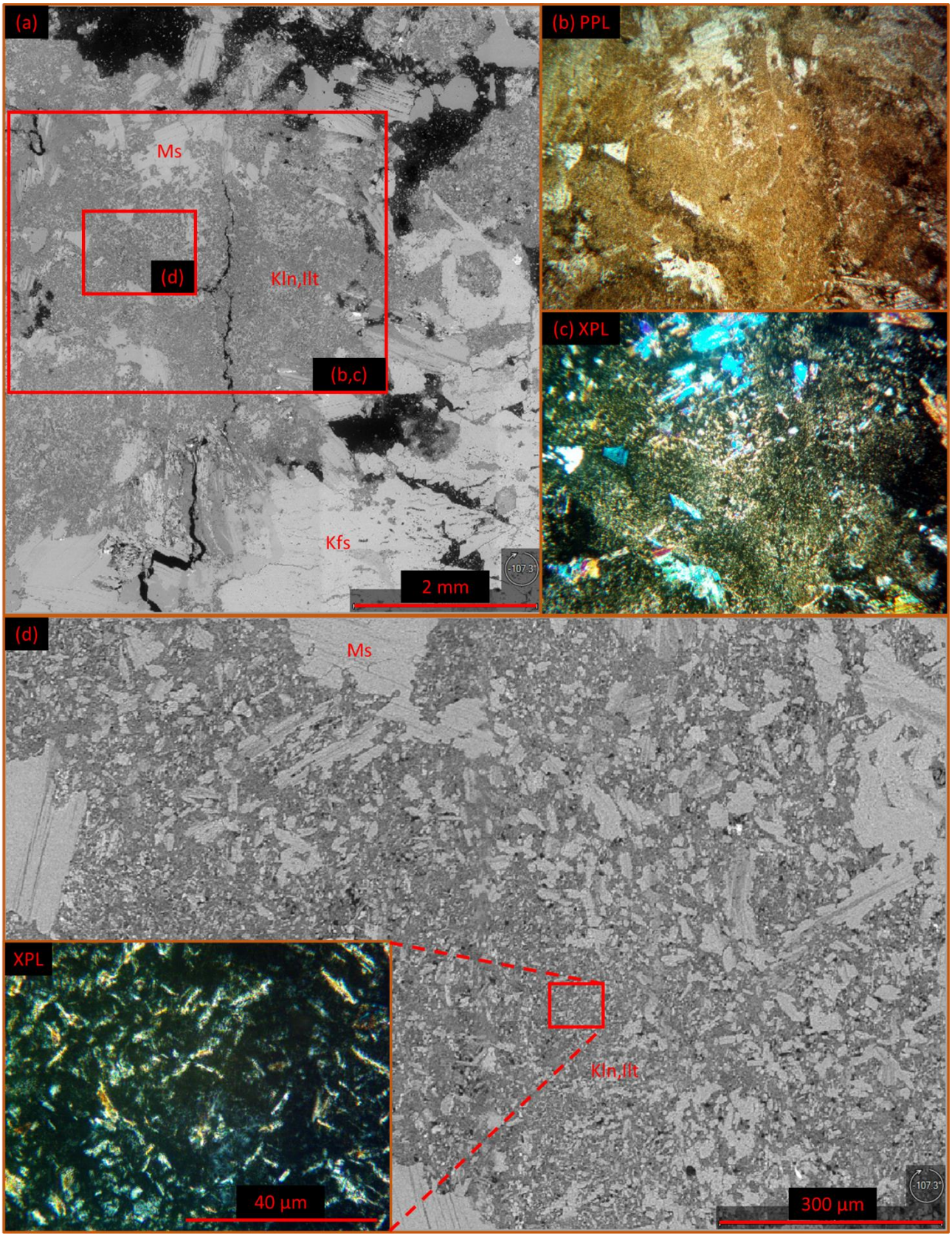

Figure 9: Microcrystalline and microporous region within altered granite. Argillic alteration of plagioclase transformed feldspar into clays. (a) overview over the region showing porosity at the top and K-Feldspar in the bottom right. (b) parallel- and (c) cross-polarised light images of the region indicating crystal distribution and effect on rock colour (brown). (d) Focus on microcrystals showing elongated (platy) clays in optical image (XPL).

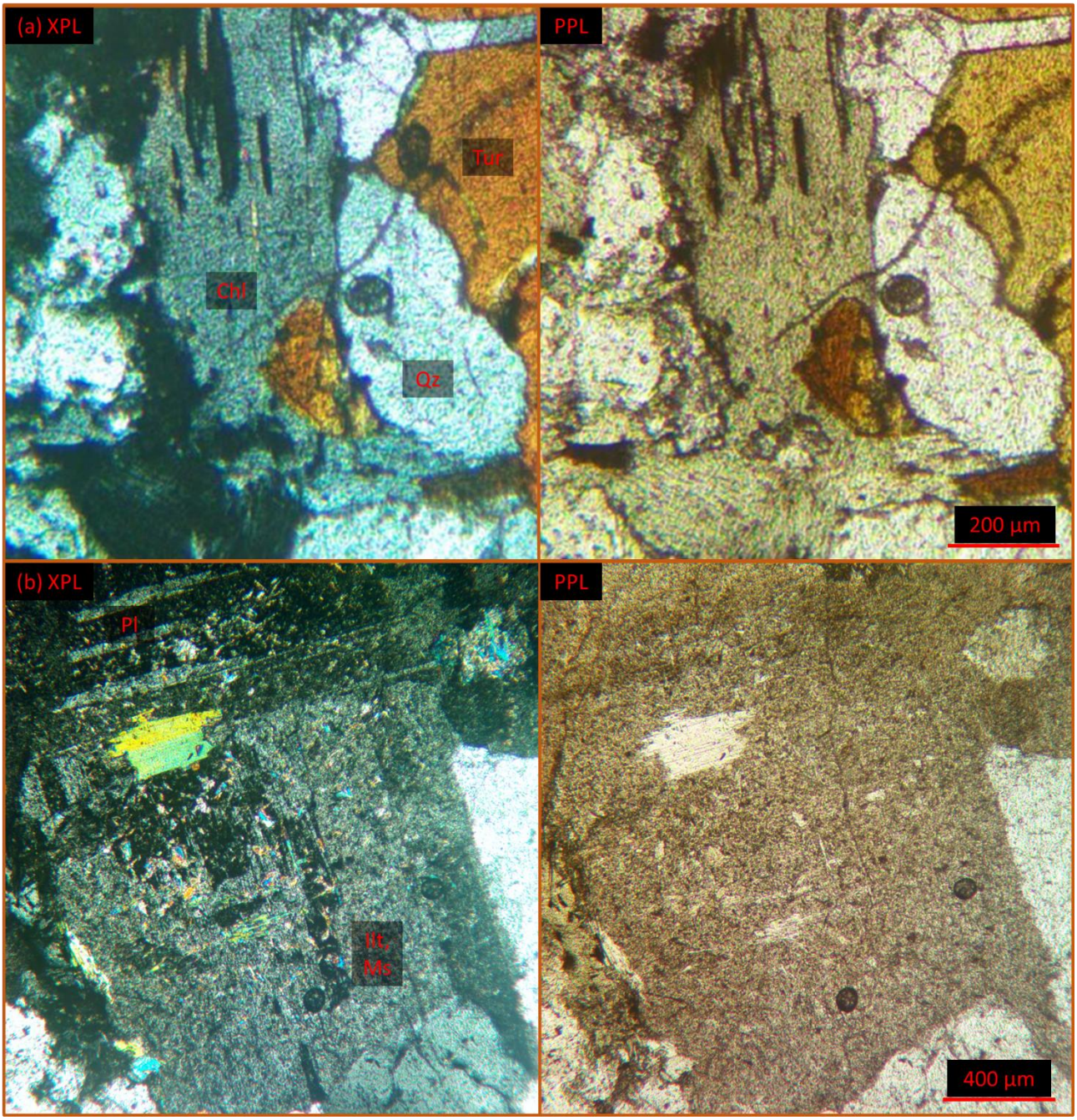

Figure 10: Optical microscopic images indicating beginning of (a) chloritisation of biotite and (b) sericitisation of plagioclase. Images taken under cross- (left) and parallel-polarised (right) light.

Insights from µ-CT analysis

To verify the interconnectivity of altered minerals within the highly altered granite, we used µ-CT analysis. Using grey scale thresholding we were able to identify the different major mineral phases, as well as fractures and void spaces within the material. Since denser materials appear brighter in CT scans, void spaces filled with air, like pores or fractures, are black and less dense material, like the altered minerals, take on darker shades of grey (see Figure 11). Our scans show that the alteration minerals occupy substantial volumes of our highly altered sample and are connected over the whole length of the sample (Figure 11 and Figure 12) thereby creating connected fluid pathways. This explains the higher matrix permeability (Figure 5) than in the slightly

343 altered granite - and we assume the unaltered granite - which are devoid of significant alteration. Further CT-
344 analysis shows that the macroscopic pores (>15 microns) only account for 1-2% porosity in the highly altered
345 sample. As NMR measurements showed approximately 10% porosity, the remaining 8-9% must be related to
346 microporosity in the altered clay-rich zones, not resolvable from our CT scans.

347 In addition to the increase in porosity through argillic alteration, tectosilicates (feldspar) are transformed into
348 phyllosilicates, which are weaker (Okrusch and Frimmel 2020). Consequently, this leads to a decrease in rock
349 strength, increasing potential for fracture formation and propagation on a grain scale. We observe this in the
350 tensile strength data, but it has also been observed in the St Austell Granite that was targeted in the Eden
351 Geothermal Project (Coggan et al. 2013). This is also supported by our CT-scans which demonstrate that the
352 induced fracture, which spans the sample, is predominantly contained within the altered minerals (Figure 11).
353 In some cases, the fracture deviates from the ideal direction (parallel to loading) and avoids splitting stronger
354 K-feldspar or quartz crystals as can be seen in xz-cut in Figure 11. In comparison, the fracture in the unaltered
355 granite propagates along grain boundaries and crosses all types of crystal, because the main minerals (quartz,
356 feldspars) are comparable in strength which is different to the altered aggregates in the highly altered sample.

357 Taking this into account we suggest that the highly altered granite, and more specifically the asperities along
358 the fracture surface, are more easily deformed under loading. This leads to a reduced fracture aperture, and
359 consequently a lower flow rate and permeability than that of the unaltered/slightly altered samples.

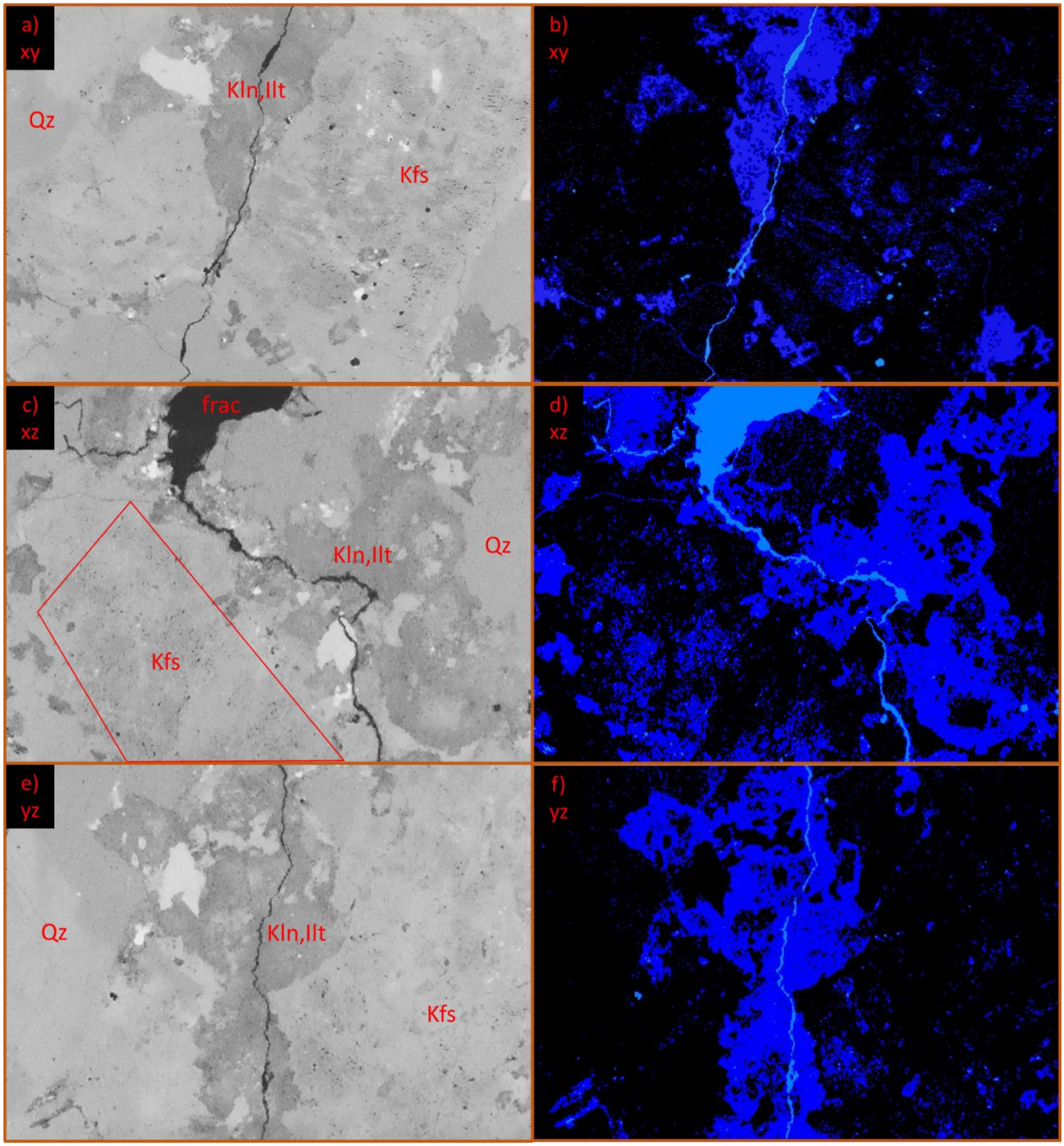

Figure 11: XRT scan images of the fractured highly altered sample. The images show cross sections in the three major planes (xy, xz and yz). The images on the left hand side (a, c, e) show the processed greyscale images, where more dense and unaltered minerals (e.g. quartz) are brighter shade of grey, less dense and altered phases (e.g. clay rich, microporous zone) are darker grey, and open spaces (e.g. fractures/large pores) are black. The right hand side (b, d, f) show the segmented images, where more dense and unaltered minerals (e.g. quartz) are black, less dense and alteration minerals (e.g. clay rich, microporous zone) are dark blue, and open spaces (e.g. fractures/large pores) are light blue. The segmented images are used to identify the connectivity of the altered, microporous regions across the material (also see Figure 12). The large fracture volume in the xz-plane is caused by a steep angle between cross-section and fracture plane making the fracture appear wider than it is. Furthermore, the position of a K-feldspar undergoing sericitisation is indicated on the xz-plane.

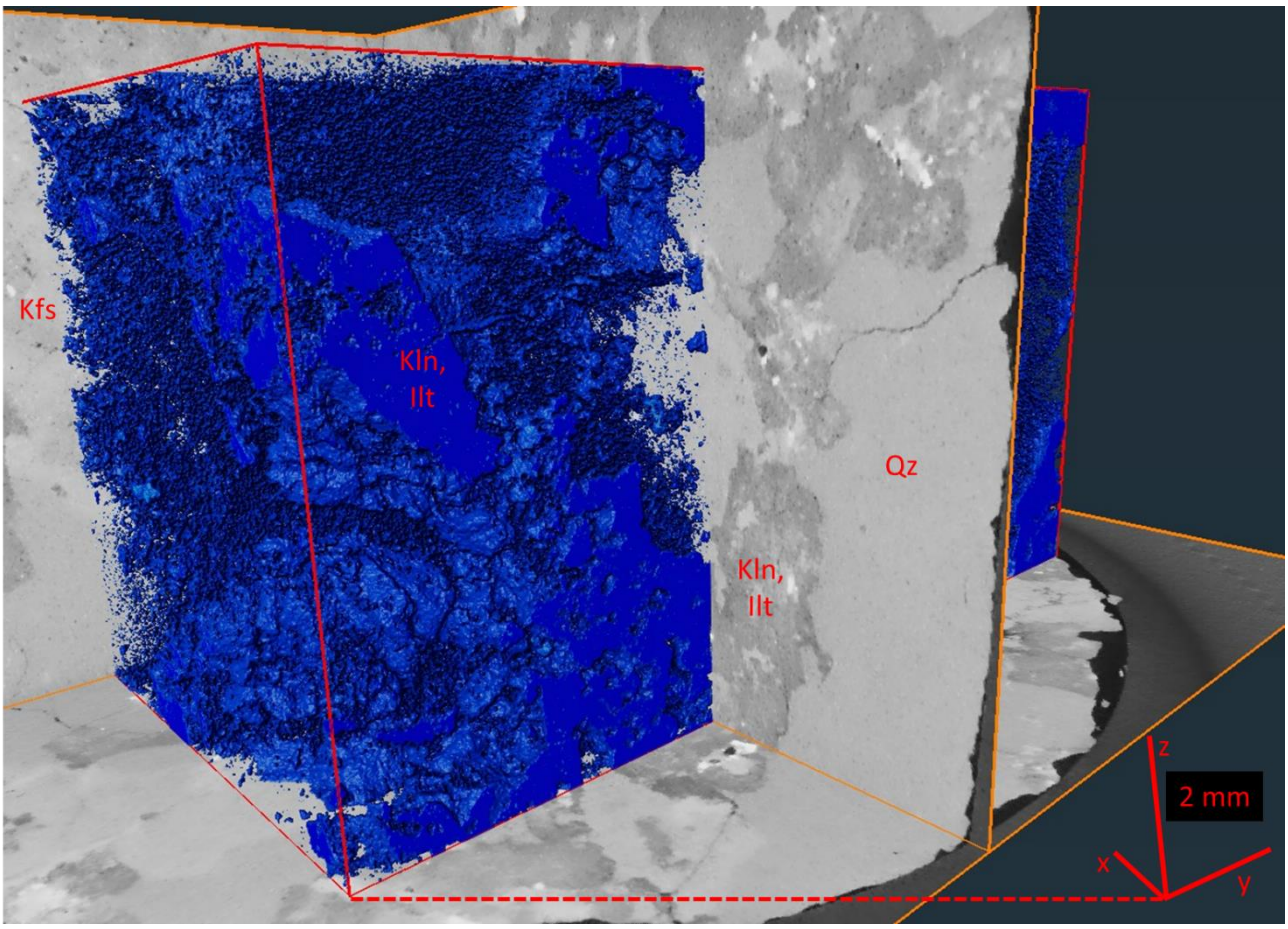

Figure 12: 3D render of the altered zones in the highly altered sample next to cross-sections of the CT-scan. Clay rich, microporous altered regions (i.e. formerly feldspars, mainly plagioclase) are indicated by the blue point clouds, while the most alteration-resistant quartz appears as void space. Using the 3D render illustrates that the clay rich, microporous regions are connected across the sample.

Implications for fluid flow

Snippe et al. (2022) describe a method to calculate the fracture aperture and fracture permeability from plug permeabilities of fractured samples. Using this method we can investigate further the effects of alteration on fracture aperture, fracture permeability, and consequently the implications for fluid flow.

Figure 13a shows the difference between the fracture aperture of the three rock types, and how this varies with effective stress. The difference between the fracture aperture calculated for the unaltered and slightly altered granites remains relatively constant across all effective stress states. In contrast, the difference between the fracture aperture calculated for the highly altered granite and the other two rock types increases with effective stress. Given that fracture aperture and fracture permeability are related through the cubic law (Snow 1969; Witherspoon *et al.* 1980; Zimmerman and Bodvarsson 1996), a similar relationship is observed for fracture permeability against effective stress (Figure 13b).

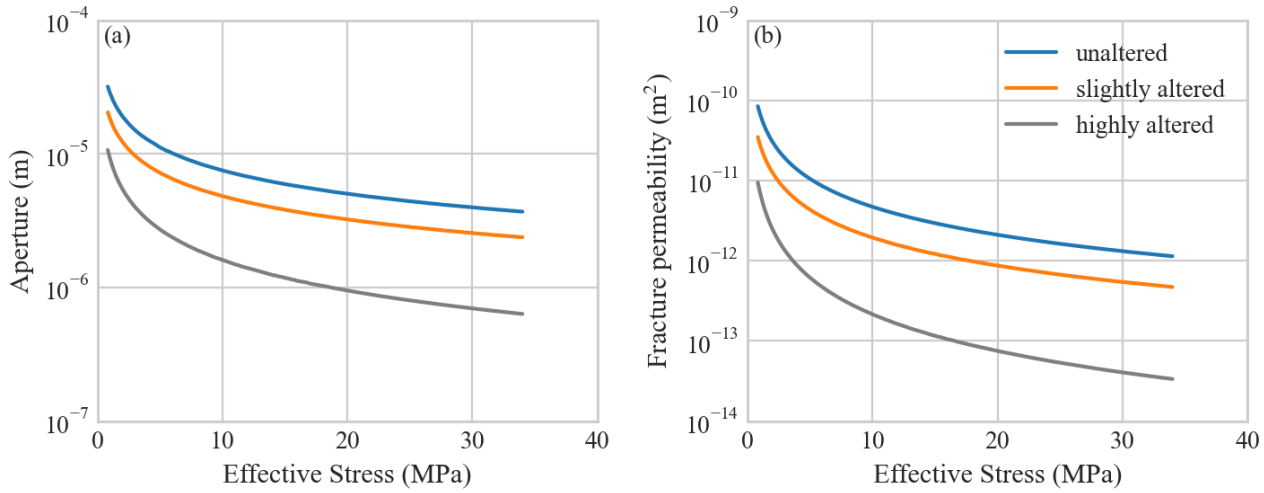

Figure 13: a) fracture aperture and b) fracture permeability against effective stress of the three rock types using the method described by Snippe et al. (2022).

The method described by Snippe et al (2020) assumes that a single macroscopic fracture spans the sample, and that fluid flow is controlled by this fracture. As has already been discussed, the fractured sample of unaltered granite contained an addition branch fracture (Figure 7). While the absolute values of fracture aperture and fracture permeability for the unaltered granite may not be accurate due to the presence of the branch fracture, a relative comparison between data from the other two rock types can be used to understand the differences in material properties and deformation mechanisms occurring within the samples. Both the data of the unaltered and slightly altered material follow the same trend with increasing effective stress i.e. the two do not diverge or converge. In contrast, the calculated fracture aperture and permeability of the highly altered granite diverges away from the data of the unaltered and slightly altered granite. This suggests that there is a fundamental difference in material properties that effects the fracture closure and permeability of the highly altered material. For the range of effective stresses that we have investigated (1 – 34 MPa) the maximum difference in fracture aperture between the slightly altered and highly altered granites is over half an order of magnitude, and the difference in fracture permeability is over an order of magnitude.

When considering fluid flow through a reservoir containing both hydrothermal alteration and fractures, understanding these differences is important (March *et al.* 2020), and they can significantly affect the long-term behaviour of a system. Unless pore fluid pressure is maintained through recharge of a system, fluid production will ultimately lead to a local decrease in effective stress. Should a significant portion of the transmissive fractures in a system be hosted within highly altered (i.e. argillic alteration) material this will lead to a more significant fracture closure than compared to fractures hosted in comparatively unaltered material, which will likely lead to lower flow rates over time. For the highly altered granite that we have used in our study the difference in plug permeabilities of the unfractured and fractured samples are approximately half an order of magnitude at the highest effective stress that we tested. It may be even smaller at higher effective stresses, where the fracture may be sufficiently closed that permeability is essentially matrix-controlled. Further investigations of this aspect fall outside this study, but we believe that these effects on long-term productivity should be considered in an upscaled reservoir modelling exercise supported by experimental data at higher

effective stresses. A dual porosity model should be used to investigate the interaction between flow in the matrix and fractures, which is another important consideration (March *et al.* 2018).

Implications for reservoir volume

The creation of porosity as a result of argillic alteration has significant implications for reservoir characteristics and on the viability of geothermal energy projects in granite-based systems. Firstly, it is important to note that zones of argillic alteration are confined to sites of previous fracture-controlled paleogeothermal fluid flow and that the width of these zones can vary from several cm to 10+ metres (Reinecker *et al.* 2021). Also, the process of alteration is gradual, and while we present data from three variably altered granites at varying distances to a fault core, these only represent a snapshot of the reservoir. Rocks closer to the fault core may be more porous and have a higher matrix permeability than those tested in this study, while those that exist (spatially) between the highly altered and slightly altered material may have porosities and matrix permeabilities between those presented in this study. It is therefore difficult to make quantitative predictions based on these data alone, but this study demonstrates how alteration may impact reservoir quality.

One of the crucial implications from this study is that of the storage potential of reservoir fluids in the altered zones. With a porosity of ~10%, the storage potential of the highly altered granite is not dissimilar to some reservoir rocks in sedimentary basins (Weedman *et al.* 1992; O'Neill *et al.* 2018). The conventional view of geothermal systems based in granite is either that they are dry (hot dry rock) and so fluids need to be introduced to the system or that fluids are hosted within existing fractures (hot wet rock). Both types are classified under Enhanced (or Engineered) Geothermal Systems (EGS) (e.g. Genter et al. 2010; Ledesert and Hebert 2012; Olasolo et al. 2016; Lu 2018; Norbeck et al. 2018). Other crystalline-hosted geothermal systems also contain mineralised fractures, which are indicative of paleogeothermal fluid migration in the past (e.g. Aquilina et al. 1997; Dezayes et al. 2005; Ledesert and Hebert 2012; Holl 2015). Consequently, it is likely that there will be some amount of hydrothermal alteration in the surrounding rock mass, as observed in the Carnmenellis Granite. The effects of hydrothermal alteration on the porosity of igneous rock has been investigated previously (e.g. Stimac et al. 2015; Mayer et al. 2016; Mordensky et al. 2018; Heap et al. 2019; Staněk and Géraud 2019). It has been demonstrated that depending on the type of alteration coupled to initial rock and fluid composition, alteration can either lead to porosity increase or decrease, and therefore it has a primary control on the storage potential of hot fluids. In the context of the granite-based systems of Cornwall, but also those in the Scottish Highlands (Roberto Rizzo, personal communication), we observe a porosity increase around cross-course fault systems and other fault orientations where substantial argillisation has locally occurred. Qualitatively it is clear that the wider the zone of alteration, the greater the increase in the storage potential in these geothermal systems. However, a simple quantitative assessment demonstrates the potential implications in terms of resource assessment.

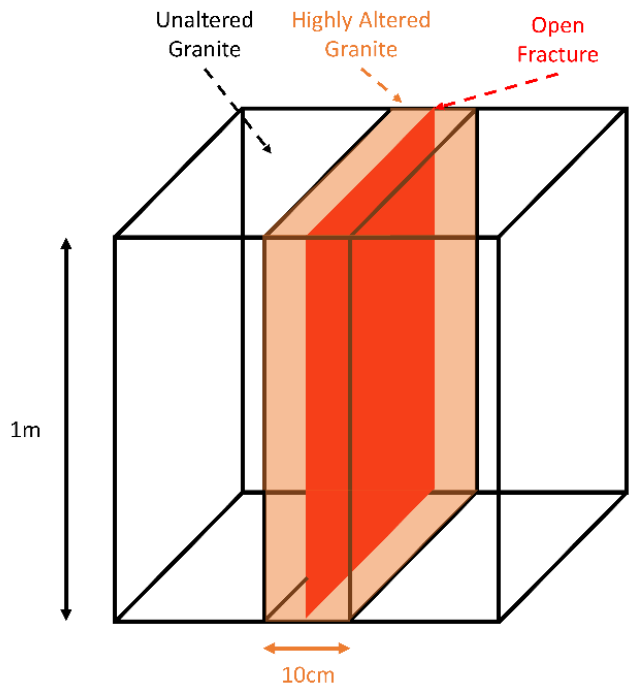

Figure 14: Conceptual drawing of *a* system containing a fracture surrounded by highly altered material, used for calculating the porosity portion ($\varphi_{portion}$) described in the text

For example, assume that the hydrothermally altered zone is 10 cm wide, with a porosity of 10% and spans the length of a single transmissive fracture which has an aperture of 0.25 mm (value taken from Heap et al. (2019). If this fracture and zone spans a volume of 1 m^3 (Figure 14), then the fracture porosity as a portion of the whole rock can be calculated according to:

$$\varphi_{portion} = \frac{length \times width \times height \times porosity}{Total\ block\ volume}$$

We assume a completely open fracture with porosity of 1, which leads to a value of $\varphi_{portion}$ of 0.00025. By using the same equation, the porosity of the hydrothermally altered zone as a portion of the whole block is 0.01, i.e. 40 times greater. This means that the altered zone can host 40 times more fluid than the fracture. In reality, the hydrothermally altered zone will vary in width (from our observations centimetres to 10+ metres) along a series of fractures within the fault zone. The fracture aperture will also vary and the porosity of the altered zone will likely vary as a function of proximity to the fault core. Furthermore, while the highly altered granite analysed in this study is permeable due to connectivity of the secondary porosity developed by dissolution-precipitation reactions accompanying argillic alteration (kaolinisation), this may not be the case for either more or less altered granite. The connected porosity is therefore also important to consider when assessing the accessible resource. However, although our analysis is simplified, it does demonstrate the implications that even a very modest amount of hydrothermal alteration may have on the overall geothermal resource.

5. Conclusions

We have measured the mineralogy, tensile strength, porosity, and permeability of samples of Carnmenellis Granite, taken from Holman's Test Mine in Cornwall. The sample material is of varying stages of argillic alteration, caused by paleogeothermal fluid flow and wall-rock alteration accompanying the development of the cross-course fault system. Three stages of alteration were evaluated: unaltered (near pristine granite), slightly altered (containing tourmaline and very minor amounts of argillic alteration) and highly altered (significant argillic alteration).

We found that the slightly altered granite is the strongest, likely due to the presence of tourmaline, and that the highly altered granite is weakest, likely due to higher porosity and clay content generated during the replacement of plagioclase feldspar. There is no significant difference between the unaltered and slightly

altered granites in terms of porosity (1-2%) and we therefore assume that the two also have comparable matrix permeabilities (~10^{-20} - 10^{-21} m^2). There is a significant difference between these two and the highly altered granite, which has a porosity of ~10% and a permeability of ~10^{-17} m^2. Using a combination of optical microscopy, SEM and XRT we demonstrate that the porous, clay rich zones, primarily resulting from plagioclase replacement, are connected across the thickness of the highly altered material, and this is likely the cause of the significantly increased permeability.

Fractured samples exhibit an increase in permeability, but when comparing the different alteration grades, the highly altered material has a lower plug permeability (~10^{-16} - 10^{-17} m^2) than the unaltered/slightly altered material (~10^{-15} m^2). We explain this by asperities along the fracture surface in the highly altered material that are weaker compared to the unaltered/slightly altered material. Therefore, this leads to a reduced aperture and consequently permeability under the same loading conditions.

Finally, we demonstrate that the accessible energy resource in granite-based geothermal energy systems, like those in Cornwall, is highly dependent on alteration zones surrounding transmissive fractured zones. Using a simple analysis, we show that depending on the porosity and thickness of the altered zone, the overall extractable resource can vary by several orders of magnitude. We therefore stress the importance of understanding the amount and type of alteration present with such geothermal systems, and its effect on the reservoir quality at an early stage of a project.

6. Acknowledgements

This work was funded through the NERC GWatt project (NE/S004769/1). We would like to thank the GWatt team (in particular Chris Rochelle, Chris Yeomans, Andrew Kilpatrick and Robert Cuss) for their help in acquiring samples, organising project meetings fruitful discussion around the study topic, Jim Buckman and Helen Lewis for their help in acquiring SEM and µ-CT data, and Paul Miller, John Fletcher and Graham Sorley for their help in sample preparation.

7. References

Abesser, C., Busby, J., Pharaoh, T., Bloodworth, A. and Ward, R. 2020. *Unlocking the Potential of Geothermal Energy in the UK Decarbonisation and Resource Management Programme*.

Aquilina, L., Pauwels, H., Genter, A. and Fouillac, C. 1997. Water-rock interaction processes in the Triassic sandstone and the granitic basement of the Rhine Graben: Geochemical investigation of a geothermal reservoir. *Geochimica et Cosmochimica Acta*, **61**, 4281–4295, https://doi.org/10.1016/S0016-7037(97)00243-3.

Artemieva, I.M., Thybo, H., Jakobsen, K., Sørensen, N.K. and Nielsen, L.S.K. 2017. Heat production in granitic rocks: Global analysis based on a new data compilation GRANITE2017. *Earth-Science Reviews*, **172**, 1–26, https://doi.org/10.1016/j.earscirev.2017.07.003.

Baba, M., Parnell, J. and Bowden, S. 2018. The geochemistry of oil in cornish granites. *Petroleum Geoscience*, **25**, 298–305, https://doi.org/10.1144/petgeo2018-053.

Batchelor, T., Curtis, R. and Busby, J. 2020. Geothermal Energy Use , Country Update for United Kingdom. *In*: *World Geothermal Congress*. 1–10.

Beamish, D. and Busby, J. 2016. The Cornubian geothermal province: heat production and flow in SW England: estimates from boreholes and airborne gamma-ray measurements. *Geothermal Energy*, **4**, https://doi.org/10.1186/s40517-016-0046-8.

Bevins, R.E., Young, B., Mason, J.S., Manning, D.A.C. and Symes, R.F. 2010. Mineralization of England and Wales. *Geological Conservation Review Series*, **36**.

Busby, J. 2010. Geothermal prospects in the United Kingdom. *Proceedings of the World Geothermal Congress*, 25–29.

Busby, J. and Terrington, R. 2017. Assessment of the resource base for engineered geothermal systems in Great Britain. *Geothermal Energy*, https://doi.org/10.1186/s40517-017-0066-z.

Busby, J., Gillespie, M. and Render, S. 2015. How hot are the Cairngorms? *Scottish Journal of Geology*, **51**, 105–115, https://doi.org/10.1144/sjg2014-027.

Carr, H.Y. and Purcell, E.M. 1954. Effects of diffusion on free precession in nuclear magnetic resonance experiments. *Physical Review*, **94**, 630–638, https://doi.org/10.1103/PhysRev.94.630.

Chadwick, R.A. and Evans, D.J. 1995. *The Timing and Direction of Permo-Triassic Extension in Southern Britain*.

Chen, Y., Clark, A.H., Farrar, E., Wasteneys, H.A.H.P., Hodgson, M.J. and Bromley, A. V. 1993. *Diachronous and Independent Histories of Plutonism and Mineralization in the Cornubian Batholith, Southwest England*.

Coggan, J.S., Stead, D., Howe, J.H. and Faulks, C.I. 2013. Mineralogical controls on the engineering behavior of hydrothermally altered granites under uniaxial compression. *Engineering Geology*, **160**, 89–102, https://doi.org/10.1016/j.enggeo.2013.04.001.

Cuss, R.J., Harrington, J.F., Sathar, S., Norris, S. and Talandier, J. 2017. Applied Clay Science The role of the stress-path and importance of stress history on the fl ow of water along fractures and faults ; an experimental study conducted on kaolinite gouge and Callovo-Oxfordian mudstone. **150**, 282–292, https://doi.org/10.1016/j.clay.2017.09.029.

Dearman, W.R. 1963. Wrench-faulting in Cornwall and south Devon. *Proceedings of the Geologists' Association*, **74**, 265–287, https://doi.org/10.1016/S0016-7878(63)80023-1.

Dezayes, C., Genter, A. and Hooijkaas, G.R. 2005. Deep-seated geology and fracture system of the EGS Soultz reservoir (France) based on recent 5km depth boreholes. *In*: *Proceedings World Geothermal Congress*. 24–29.

Dines, H. 1956. *The Metalliferous Mining Region of South-West England*.

Eden Geothermal Limited. 2023. The Eden Geothermal Project. *https://www.edengeothermal.com/the-project/*https://www.edengeothermal.com/the-project/.

Faulkner, D.R., Jackson, C.A.L., Lunn, R.J., Schlische, R.W., Shipton, Z.K., Wibberley, C.A.J. and Withjack, M.O. 2010. A review of recent developments concerning the structure, mechanics and fluid flow properties of fault zones. *Journal of Structural Geology*, **32**, 1557–1575, https://doi.org/10.1016/j.jsg.2010.06.009.

Fink, R., Krooss, B.M., Gensterblum, Y. and Amann-Hildenbrand, A. 2017. Apparent Permeability of Gas Shales - Separation of Fluid-Dynamic and Poro-Elastic Effects. *Fuel*, **199**, 532–550, https://doi.org/10.1061/9780784480779.239.

564 Forbes Inskip, N., Phillips, T., et al. 2022. Linking Fracture Roughness and Orientation to Bedding : Impact on
565 Fluid Flow. *Earth and Space Science Open Archive*, 1–21.

566 Genter, A., Evans, K., Cuenot, N., Fritsch, D. and Sanjuan, B. 2010. Contribution of the exploration of deep
567 crystalline fractured reservoir of Soultz to the knowledge of enhanced geothermal systems (EGS).
568 *Comptes Rendus - Geoscience*, **342**, 502–516, https://doi.org/10.1016/j.crte.2010.01.006.

569 Gleeson, S.A., Wilkinson, J.J., Shaw, H.F. and Herrington, R.J. 2000. *Post-Magmatic Hydrothermal Circulation*
570 *and the Origin of Base Metal Mineralization, Cornwall, UK Background Geology*.

571 Gluyas, J.G., Adams, C.A., et al. 2018. Keeping warm: a review of deep geothermal potential of the UK.
572 *Proceedings of the Institution of Mechanical Engineers, Part A: Journal of Power and Energy*, **232**, 115–
573 126, https://doi.org/10.1177/0957650917749693.

574 Gudmundsson, A. 2011. *Rock Fractures in Geological Processes*.

575 Harpers, N., Forbes Inskip, N., Allen, M.J., Faulkner, D., Claes, H., Busch, A. and Den Hartog, S. 2022. Direct
576 shear experiments to investigate the effect of chemical alteration on fault frictional behaviour in
577 granitic geothermal systems. *In*: *European Geosciences Union, General Assembly* ,
578 https://doi.org/10.5194/egusphere-egu22-12855.

579 Harvey, C., Beardsmore, G., Moeck, I. and Ruter, H. 2016. *Geothermal Exploration: Global Strategies and*
580 *Applications*.

581 Heap, M.J., Gravley, D.M., Kennedy, B.M., Gilg, H.A., Bertolett, E. and Barker, S.L.L. 2019. Quantifying the
582 role of hydrothermal alteration in creating geothermal and epithermal mineral resources: The Ohakuri
583 ignimbrite (Taupō Volcanic Zone, New Zealand). *Journal of Volcanology and Geothermal Research*,
584 **390**, 106703, https://doi.org/10.1016/j.jvolgeores.2019.106703.

585 Holl, H.-G. 2015. *What Did We Learn about EGS in the Cooper Basin?*,
586 https://doi.org/10.13140/RG.2.2.33547.49443.

587 Holloway, S. and Chadwick, R.A. 1986. *The Sticklepath-Lustleigh Fault Zone: Tertiary Sinistral Reactivation of*
588 *a Variscan Dextral Strike-Slip Fault*.

589 Houben, M.E., Eeden, J.C.M. van, Barnhoorn, A. and Hangx, S.J.T. 2020. Fracture-Induced Permeability in
590 Whitby Mudstone. *Environmental Science & Technology*, https://doi.org/10.1021/acs.est.0c00557.

591 ISRM. 1978. Suggested Methods For Determining Tensile Strength of Rock Materials. *International Journal*
592 *of Rock Mechanics and Mining Sciences and Geomechanics*, **15**, 99–103,
593 https://doi.org/10.1016/0148-9062(78)90003-7.

594 Klinkenberg, L.J. 1941. The permeability of porous media to liquids and gases. *Drilling and Production*
595 *Practice 1941*, 200–213.

596 Ledesert, B.A. and Hebert, R.L. 2012. The Soultz-sous-Forêts' Enhanced Geothermal System: A Granitic
597 Basement Used as a Heat Exchanger to Produce Electricity. *Heat Exchangers - Basics Design*
598 *Applications*, https://doi.org/10.5772/34276.

599 Ledingham, P., Cotton, L. and Law, R. 2019. The United Downs Deep Geothermal Power Project.
600 *PROCEEDINGS 44th Workshop on Geothermal Reservoir Engineering*, 1–11.

601 Lu, S.-M. 2018. A global review of enhanced geothermal system (EGS). *Renewable and Sustainable Energy*
602 *Reviews*, **81**, 2902–2921, https://doi.org/https://doi.org/10.1016/j.rser.2017.06.097.

March, R., Doster, F. and Geiger, S. 2018. Assessment of CO2 Storage Potential in Naturally Fractured Reservoirs With Dual-Porosity Models. *Water Resources Research*, **54**, 1650–1668, https://doi.org/10.1002/2017WR022159.

March, R., Egya, D., Maier, C., Busch, A. and Doster, F. 2020. Numerical computation of stress-permeability relationships of fracture networks in a shale rock.

Mayer, K., Scheu, B., Montanaro, C., Yilmaz, T.I., Isaia, R., Aßbichler, D. and Dingwell, D.B. 2016. Hydrothermal alteration of surficial rocks at Solfatara (Campi Flegrei): Petrophysical properties and implications for phreatic eruption processes. *Journal of Volcanology and Geothermal Research*, **320**, 128–143, https://doi.org/10.1016/j.jvolgeores.2016.04.020.

Mccay, A.T. and Younger, P.L. 2017. Ranking the geothermal potential of radiothermal granites in Scotland: are any others as hot as the Cairngorms?, https://doi.org/10.5525/gla.researchdata.302.

Meiboom, S. and Gill, D. 1958. Modified spin-echo method for measuring nuclear relaxation times. *Review of Scientific Instruments*, **29**, 688–691, https://doi.org/10.1063/1.1716296.

Moore, C.H. and Wade, W.J. 2013. Natural fracturing in carbonate reservoirs. *In*: *Developments in Sedimentology*. 285–300., https://doi.org/10.1016/B978-0-444-53831-4.00011-2.

Mordensky, S.P., Villeneuve, M.C., Kennedy, B.M., Heap, M.J., Gravley, D.M., Farquharson, J.I. and Reuschlé, T. 2018. Physical and mechanical property relationships of a shallow intrusion and volcanic host rock, Pinnacle Ridge, Mt. Ruapehu, New Zealand. *Journal of Volcanology and Geothermal Research*, **359**, 1–20, https://doi.org/10.1016/j.jvolgeores.2018.05.020.

Nishimoto, S. and Yoshida, H. 2010. Hydrothermal alteration of deep fractured granite: Effects of dissolution and precipitation. *Lithos*, **115**, 153–162, https://doi.org/10.1016/j.lithos.2009.11.015.

Norbeck, J.H., McClure, M.W. and Horne, R.N. 2018. Field observations at the Fenton Hill enhanced geothermal system test site support mixed-mechanism stimulation. *Geothermics*, **74**, 135–149, https://doi.org/10.1016/j.geothermics.2018.03.003.

Okrusch, M. and Frimmel, H.E. 2020. *Mineralogy*, 1st ed., https://doi.org/https://doi.org/10.1007/978-3-662-57316-7.

Olasolo, P., Juárez, M.C., Morales, M.P., Damico, S. and Liarte, I.A. 2016. Enhanced geothermal systems (EGS): A review. *Renewable and Sustainable Energy Reviews*, **56**, 133–144, https://doi.org/10.1016/j.rser.2015.11.031.

O'Neill, S.R., Jones, S.J., Kamp, P.J.J., Swarbrick, R.E. and Gluyas, J.G. 2018. Pore pressure and reservoir quality evolution in the deep Taranaki Basin, New Zealand. *Marine and Petroleum Geology*, **98**, 815–835, https://doi.org/10.1016/j.marpetgeo.2018.08.038.

Phillips, T., Kampman, N., Bisdom, K., Forbes Inskip, N.D., den Hartog, S.A.M., Cnudde, V. and Busch, A. 2020. Controls on the intrinsic flow properties of mudrock fractures: A review of their inportance in subsurface storage. *Earth Science Reviews*, **210**, https://doi.org/10.1016/j.earscirev.2020.103390.

Pine, R.J. and Batchelor, A.S. 1984. Downward migration of shearing in jointed rock during hydraulic injections. *International Journal of Rock Mechanics and Mining Sciences and*, **21**, 249–263, https://doi.org/10.1016/0148-9062(84)92681-0.

Reinecker, J., Gutmanis, J., Foxford, A., Cotton, L., Dalby, C. and Law, R. 2021. Geothermal exploration and reservoir modelling of the united downs deep geothermal project, Cornwall (UK). *Geothermics*, **97**, 102226, https://doi.org/10.1016/j.geothermics.2021.102226.

Rollin, K.E. 1982. *A Review of Data Relating to Hot Dry Rock and Selection of Targets for Detailed Study. Report in Series: Investigation of the Geothermal Potential of the UK*.

Rushing, J.A., Corp, A.P., Newsham, K.E., Corp, A., Lasswell, P.M. and Laboratories, O. 2004. SPE 89867 Klinkenberg-Corrected Permeability Measurements in Tight Gas Sands : Steady-State Versus Unsteady-State Techniques.

Shail, R. and Alexander, A. 1997. Late Carboniferous to Triassic reactivation of Variscan basement in the western English Channel: evidence from onshore exposures in south Cornwall. *Journal of the Geological Society, London*, **154**, 163–168.

Simons, B., Shail, R.K. and Andersen, J.C.O. 2016. The petrogenesis of the Early Permian Variscan granites of the Cornubian Batholith: Lower plate post-collisional peraluminous magmatism in the Rhenohercynian Zone of SW England. *Lithos*, **260**, 76–94, https://doi.org/10.1016/j.lithos.2016.05.010.

Snippe, J., Kampman, N., et al. 2022. Modelling of long-term along-fault flow of CO2 from a natural reservoir. *International Journal of Greenhouse Gas Control*, **118**, 103666, https://doi.org/10.1016/j.ijggc.2022.103666.

Snow, D.T. 1969. Anisotropie Permeability of Fractured Media. *Water Resources Research*, **5**, 1273–1289, https://doi.org/10.1029/WR005i006p01273.

Span, R., Lemmon, E.W., Jacobsen, R.T., Wagner, W. and Yokozeki, A. 2000. A reference equation of state for the thermodynamic properties of nitrogen for temperatures from 63.151 to 1000 K and pressures to 2200 MPa. *Journal of Physical and Chemical Reference Data*, **29**, 1361–1401, https://doi.org/10.1063/1.1349047.

Staněk, M. and Géraud, Y. 2019. Granite microporosity changes due to fracturing and alteration: Secondary mineral phases as proxies for porosity and permeability estimation. *Solid Earth*, **10**, 251–274, https://doi.org/10.5194/se-10-251-2019.

Stimac, J., Goff, F. and Goff, C.J. 2015. Intrusion-Related Geothermal Systems. *In*: *The Encyclopedia of Volcanoes*. 799–822., https://doi.org/10.1016/b978-0-12-385938-9.00046-8.

Ulusay, R. 2014. *The ISRM Suggested Methods for Rock Characterization , Testing and Monitoring :* Ulusay, R. (ed.).

Warr, L.N. 2021. IMA–CNMNC approved mineral symbols. *Mineralogical Magazine*, **85**, 291–320, https://doi.org/10.1180/mgm.2021.43.

Weedman, S.D., Brantley, S.L. and Albrecht, W. 1992. Secondary compaction after secondary porosity: Can it form a pressure seal? *Geology*, **20**, 303–306.

Witherspoon, P.A., Wang, J.S.Y., Iwai, K. and Gale, J.E. 1980. Validity of Cubic Law for fluid flow in a deformable rock fracture. *Water Resources Research*, **16**, 1016–1024, https://doi.org/10.1029/WR016i006p01016.

Zimmerman, R.W. and Bodvarsson, G.S. 1996. Hydraulic conductivity of rock fractures. *Transport in Porous Media*, **23**, 1–30, https://doi.org/10.1007/BF00145263.

684